RESEARCH ARTICLE

Running Head: Motor unit alterations with muscle disuse

Twenty-One Days of Bed Rest Alter Motor Unit Properties and Neuromuscular Junction Transmission in Young Adults

Fabio Sarto[1,2], Miloš Kalc[3], Evgeniia S. Motanova[1], Martino V. Franchi[1,4], Daniel Stashuk[5], Nina Murks[6], Giacomo Valli[7], Samuele Negro[1], Tomaž Prašnikar[8], Mladen Gasparini[8], Giovanni Martino[1], Giuseppe De Vito[1,4], Aleš Holobar[6], Boštjan Simunič[3], Rado Pišot[3], and Marco V. Narici[1,3,4]

[1] Department of Biomedical Sciences, University of Padova, Padova, Italy

[2] Centre of Studies and Activities for Space "Giuseppe Colombo", University of Padova, Padova, Italy

[3] Science and Research Center Koper, Institute for Kinesiology Research, Koper, Slovenia

[4] CIR-MYO Myology Center, University of Padova, Padova, Italy

[5] Department of Systems Design Engineering, University of Waterloo, Ontario, Canada

[6] Faculty of Electrical Engineering and Computer Science, University of Maribor, Maribor, Slovenia

[7] Department of Clinical and Experimental Sciences, University of Brescia, Brescia, Italy

[8] Izola General Hospital, Izola, Slovenia

Correspondence: Dr. Fabio Sarto, Department of Biomedical Sciences, University of Padova, Padova, Italy; Centre of Studies and Activities for Space "Giuseppe Colombo", University of Padova, Padova, Italy – Email: fabio.sarto@unipd.it; Phone number: +39 0498275309 – ORCID: https://orcid.org/0000-0001-8572-5147

Downloaded from journals.physiology.org/journal/jappl (193.002.022.014) on May 13, 2025.

ABSTRACT

Previous studies showed that properties of higher-threshold motor units (MUs) and neuromuscular junction (NMJ) function are preserved during short-term disuse. This study aimed to test how a longer disuse period affects MU properties, NMJ transmission, and NMJ morphology remodeling. Nine young healthy males (age: 18-29 years) underwent 21 days of horizontal bed rest. Pre- (BR0) and post-bed rest (BR21), quadriceps maximal voluntary contraction (MVC), and size were assessed. We combined intramuscular electromyography (iEMG) and high-density surface electromyography (HDsEMG) recordings on the vastus lateralis to assess MU properties at 25% and 50% of MVC. Muscle biopsies and blood samples were also collected. Quadriceps MVC and size decreased at BR21. We found alterations in MU properties at both contraction intensities, including reduced discharge rate, MU potential area changes, and increased complexity. NMJ transmission was found to be reduced at BR21 at 25% MVC. This functional NMJ impairment was biochemically corroborated by an increase in serum C-terminal agrin fragment concentration, a biomarker of NMJ instability. In addition, a direct assessment of NMJ morphology revealed the presence of some denervated NMJs exclusively at BR21. In conclusion, 21-day bed rest altered MU properties across different contraction intensities and impaired NMJ transmission with initial signs of remodeling/denervation. Disuse duration appears to be a critical factor, as previous shorter studies failed to detect some of these changes. We believe these findings are clinically relevant for disuse after trauma, surgery, or illness, and may support the development of effective countermeasures.

NEW & NOTEWORTHY

Leveraging both intramuscular and high-density surface EMG recordings in the vastus lateralis, we identified alterations in motor unit (MU) properties in young adults after 21 days of bed rest. These included reduced discharge rates and changes in MU potential size and complexity, observed at both low and moderate contraction intensities. Evidence of impaired neuromuscular junction (NMJ) function and denervation was also found. Our findings indicate that medium-term disuse elicits MU-level changes not detected in shorter-duration studies.

Keywords: Disuse; Unloading; Physical inactivity; Electrophysiology; Electromyography

Downloaded from journals.physiology.org/journal/jappl (193.002.022.014) on May 13, 2025.

1. INTRODUCTION

Nearly all individuals, at some stage in life, would face periods of muscle disuse, often due to trauma, surgery, or illness. Disuse profoundly disrupts the neuromuscular system, leading to marked reductions in whole muscle size and strength (1–3). Investigating changes in motor units (MUs), the smallest functional units of the neuromuscular system (4), is of physiological and clinical significance in this scenario. From a biological perspective, all components of a MU are affected by muscle disuse: (i) muscle fibers atrophy, changing mechanical properties and proteomic profile (5–7); (ii) neuromuscular junctions (NMJs) show biochemical perturbation (8, 9); and (iii) the motoneuron sustain structural damage—although this evidence comes from animal models (10, 11). However, these changes do not necessarily imply MU functional impairment. For this reason, the plasticity of human MUs following muscle disuse has also been assessed through an in vivo evaluation of their electrophysiological properties (12, 13).

Pioneering studies detected reduced MU discharge rates (DR) in small muscles of the human hand following periods of cast immobilization (14–16). More recently, studies using state-of-the-art intramuscular electromyography (iEMG) (9, 17) and high-density surface electromyography (HDsEMG) (18, 19) have expanded these previous findings including large muscles of the lower limb, relevant for mobility and the performance of daily motor tasks. Interestingly, a recent investigation from our group (19), reported that short-term disuse (10 days of unilateral lower limb suspension) induced alterations of MU properties in the vastus lateralis, reducing DR at 25% MVC but not at 50% MVC. This may reflect a specific impairment of lower-threshold MUs with short-term disuse. Whether higher-threshold MUs are also impaired by longer periods of muscle disuse remains unknown. This is particularly relevant, as higher-threshold MUs are crucial for generating maximal muscle force (20, 21) and are predominantly recruited during high-intensity activities (22), such as moving heavy weights, climbing stairs rapidly, jumping, and recovering balance to avoid falls.

Another interesting finding from recent studies is that human NMJ function, assessed electrophysiologically *in vivo* by iEMG, was preserved during short periods of disuse (10-15 days) (9, 17). This finding is surprising, especially considering NMJ instability with muscle disuse in humans was previously inferred through circulating and muscle biomarkers (8, 9).

Downloaded from journals.physiology.org/journal/jappl (193.002.022.014) on May 13, 2025.

We previously proposed that NMJs may be only transiently resilient from a functional perspective in conditions of muscle disuse (9) but this hypothesis has never been verified. Considering that the duration of these previous studies may have not been sufficient to trigger this electrophysiological impairment, we aimed to establish whether a longer period of muscle disuse would affect MUs properties and NMJ transmission at both low and moderate contraction intensities in young adults. To address this question, we employed the bed rest model, the gold-standard approach for experimentally studying muscle disuse, for 21 days. To investigate these aspects comprehensively, we leveraged a novel set-up enabling the simultaneous collection of iEMG and HDsEMG recordings, complemented by biochemical and morphological NMJ evaluation. We hypothesize that medium-term bed rest impairs MU properties across different contraction intensities, and induces alterations in NMJ structure and function.

2. MATERIALS AND METHODS

2.1 Ethical approval

The present study was carried out in line with the latest revision of the Declaration of Helsinki and was approved by the National Ethical Committee of the Slovenian Ministry of Health with reference number 0120-123/2023/9. The research team thoroughly informed the participants about the experimental procedures via an interview and an information sheet. Written informed consent was obtained from all participants, who were allowed to withdraw from the study at any point.

2.2 Participants

Nine young healthy males (baseline age: 22.8 (4.4) years; height: 1.83 (0.06) m; body mass: 79.1 (6.7) kg) volunteered in this study. Only male individuals were recruited due to the higher absolute risk of a first deep venous thrombosis event in young women compared to men (23), a risk that is exacerbated by prolonged inactivity. Participants underwent medical screening before the study. The exclusion criteria were as follows: regular smoking, habitual use of drugs, disorders affecting blood clotting, a history of deep vein thrombosis with D-dimer levels above 500 µg L–1, acute or chronic conditions involving the skeletal, neuromuscular, or cardiovascular systems, metabolic diseases with associated

Downloaded from journals.physiology.org/journal/jappl (193.002.022.014) on May 13, 2025.

complications, a prior embolism, inflammatory conditions, psychiatric illnesses, epilepsy, professional-level involvement in sport, and the presence of ferromagnetic implants.

2.3 Experimental protocol

The participants underwent 21 days of horizontal bed rest, considered a medium-term duration (24). Baseline measurements (BR0) included (i) a full *in vivo* neuromuscular assessment conducted two days before the onset of bed rest, (ii) a blood sample and a muscle biopsy collected just before the bed rest initiation, and (iii) a magnetic resonance imaging (MRI) scan of thigh muscles after 8 hours of bed rest. Post-measurements (BR21) included a biopsy and MRI completed on the last day of bed rest and all the other measurements performed on the first day of recovery, with the *in vivo* tests carried out approximately 3 h after the participants stood up.

2.4 Bed rest

The study was conducted in August and September 2023 at the General Hospital of Izola (Izola, Slovenia). The participants were accommodated in standard air-conditioned hospital rooms. Twenty-four-hour medical supervision was provided, and room video surveillance was used for assistance and to monitor for any elevated positions. During the bed rest period, participants performed all daily activities while remaining strictly horizontal, using only one pillow for head support, with no deviations permitted. Participants were not allowed to engage in systematic voluntary movements or exercise-like activities during this period, although they were permitted to change positions from prone to supine if needed. Participants were served meals four times per day, adhering to a eucaloric diet with a macronutrient distribution of 60% carbohydrates, 25% fats, and 15% proteins. Water consumption was permitted ad libitum. Participants were invited to sleep between 22:00 and 07:00.

2.5 *In-vivo* muscle structure and function

Muscle strength and activation capacity

Knee extensors maximal voluntary contraction (MVC) of the right leg was assessed by isometric dynamometry fitted with a load cell (RS 206-0290; Tedea Huntleigh, Selb, Germany) at a 90° knee angle, as previously described (8, 19). We instructed the participants to push as strong and as fast as possible for 3-4s. After a warm-up consisting of 10 short sub-maximal contractions, the participants performed 3 trials, with 1 min rest

Downloaded from journals.physiology.org/journal/jappl (193.002.022.014) on May 13, 2025.

between sets. Visual feedback and loud verbal encouragement were provided during the test. The force signal was recorded at a sampling rate of 1000 Hz using LabChart software (v.8.13, ADInstrument, Dunedin, NewZealand). The maximal value reached during these trials was considered for data analysis. The MVC was then divided by the quadriceps mid-thigh CSA (see below) to obtain the knee extensors' specific tension. Activation capacity was assessed using the interpolated twitch technique. Supramaximal stimulations were delivered (stimulator: Digitimer DS7AH, Digitimer Ltd, Welwyn Garden, Hertfordshire, UK) via two 110 × 180mm pads (Axion, Leonberg, Germany) during MVC contractions. The stimulation consisted of two supra-maximal doublets (interstimulus interval 10ms): the first applied during the maximal contraction plateau and the second doublet, 1 s post-contraction at rest. The supra-maximal current was determined by increasing the current until no further force increase was observed. Activation capacity was calculated using the equation:

$$\textit{Activation Capacity} = (1 - (A/B)) \times 100$$

where A is the superimposed twitch torque and B is the resting control twitch torque.

Muscle size assessment by magnetic resonance imaging

MRI scans were collected using a 3T scanner (Magnetom Vida Fit, Siemens Healthineers, Erlangen, Germany). Participants started the bed rest period at least 8 hours before the MRI assessment, allowing for stabilization of body fluid. Turbo spin-echo T1-weighted images of both thighs were acquired in the axial plane. The acquisition parameters were as follows: sequence: Dixon, slice thickness: 5 mm, readout bandwidth: 500 Hz/pixel, voxel size: 1.1 x 1.1 x 5.0 mm, with no gap between slices, TR/TE: 550/9.80 ms, flip angle: 90°, field of view: 400 x 225 kHz. The analysis of muscle CSA was carried out for the whole quadriceps femoris and the vastus lateralis individually at 50% of femur length (distance between greater trochanter to the mid-patellar point), identified on the scans using a cod liver oil capsule as a marker. Borders of the muscles were manually outlined using Horos image analysis software (https://horosproject.org/). Data analysis was based on the average CSA obtained from three scans around 50% femur length: the primary scan marked by the cod liver oil capsule and one scan immediately above and one below this level.

2.6 *In-vivo* assessment of motor unit properties (iEMG and HDsEMG)

Downloaded from journals.physiology.org/journal/jappl (193.002.022.014) on May 13, 2025.

To comprehensively assess MU properties *in vivo*, we adopted a set-up that combines the simultaneous recording of iEMG and HDsEMG signals from the vastus lateralis. Vastus lateralis was chosen because it is a large, functional muscle involved in locomotion and independence in daily tasks, exhibits significant plasticity and atrophy during disuse (1, 2), has been studied in previous research on motor unit properties (9, 19), and is a common and safe site for muscle biopsies, facilitating to relate electrophysiological parameters to NMJ morphological analysis.

Set-up preparation

A matrix of 64 equally spaced electrodes (13 x 5, 8mm I.E.D., GR08MM1305; OT Bioelettronica, Torino, Italy) was employed for HDsEMG recordings. The matrix was disinfected with surgical disinfectant. The matrix was cut in the center with a sterile scalpel, creating a small rectangular opening (approximately 5 mm in length and 3 mm in width) for the concentric iEMG needle insertion (Fig. 1A). Caution was taken to avoid cutting the matrix circuits. The matrix was then filled with conductive paste (Ten20; Weaver and Company, Aurora, CO, USA) and attention was paid to having no contamination of conductive cream in the region where the needle would be inserted (that region remained covered during the paste application). The distal innervation zone of the vastus lateralis was identified by delivering low-intensity percutaneous electrical stimulations (8–16 mA; pulse width: 100 µs) using a pen electrode in the region between 35% and 20% of femur length, with a Digitimer DS7AH stimulator (Welwyn Garden, Hertfordshire, UK) (25). After identifying the motor point, the current was lowered to 8–10 mA to confirm it as the most responsive site, indicated by the largest evoked twitch. The skin of the participants was shaved in the area of interest and then prepared with an abrasive-conductive paste (Spes Medica, Salerno, Italy). The matrix was then placed with the central electrodes of the last 2 rows over the innervation zone, following the muscle fascicle orientation determined by B-mode ultrasonography (19). A 25 mm concentric needle electrode (S53155, Teca Elite, Natus Medical Inc., Middleton, WI, USA) was then inserted diagonally (~45°) in the rectangular opening for iEMG recordings (Fig. 1B), after disinfection with an antiseptic. The distance between the point of insertion and the innervation zone was ~36 mm. Reference electrodes for both recording systems were placed on the malleolus, patella, and patellar tendon.

Simultaneous iEMG and HDsEMG recording

Downloaded from journals.physiology.org/journal/jappl (193.002.022.014) on May 13, 2025.

Participants were asked to perform 6 trapezoidal contractions at 25% MVC and 3 at 50% MVC in alternating order, with the additional 3 contractions at 25% MVC completed at the end of the protocol. This number of contractions at 25% MVC aligns with previous iEMG studies (9, 26, 27), while fewer contractions were performed at 50% MVC to minimize muscle fatigue. Each contraction lasted 30s, with force change in the ramp-up and ramp-down phases set at 5%/s (Fig. 1C). A visual feedback was provided. A 30-second rest period was allowed after contractions at 25% MVC, while a 60-second rest period was given following contractions at 50% MVC. The needle electrode was repositioned in the muscle between each contraction by adjusting its depth, angle, and rotation. At each new position, participants were instructed to perform a low-intensity contraction, and the iEMG signal was checked for adequate sharpness (9, 28). The iEMG signal was sampled at 40 kHz using the PowerLab acquisition toolbox and the LabChart software (v.8.13, ADInstruments, Sydney, Australia). The HDsEMG signal was sampled at 2048 Hz with the 16-bit multichannel Quattrocento amplifier using the OTBioLab+ software (OT Bioelettronica, Torino, Italy), captured using a monopolar configuration, amplified by a factor of 150, and band-pass filtered at a frequency range of 10 to 500 Hz at the source. At the end of the session at BR0, the matrix position was drawn with a permanent marker and re-marked daily allowing precise repositioning of the electrode at BR21.

HDsEMG signal decomposition, analysis, and tracking

The raw monopolar HDsEMG signals were decomposed offline (MATLAB, R2023a, MathWorks Inc., MA) into MU pulse trains by a Convolution Kernel Compensation (CKC) algorithm implemented in the DEMUSE application (v.6, Maribor, Slovenia) (29). The reader is referred to previously published works for further details on the mathematical approach to the CKC method (29, 30). Briefly, blind source separation algorithms, such as the CKC method, invert the EMG mixing model and estimate the so-called MU filters. The MU filter is a unique, MU-specific set of weights in the linear spatiotemporal combination of the HDsEMG channels that yields the estimation of the individual MU spike train (31). Signals from each contraction were decomposed independently. An expert operator (M.K.) visually inspected and iteratively optimized MU filters using previously described procedures (32). Since more than one contraction per intensity (25 and 50% MVC) and time point (BR0 and BR21) were available, the contraction that yielded the highest number of MUs exhibiting a pulse-to-noise ratio ≥28 dB was retained (30) and further analyzed. Special attention has

Downloaded from journals.physiology.org/journal/jappl (193.002.022.014) on May 13, 2025.

been paid to MUs with PNR <30 dB, carefully assessing their discharge features and reasons for low PNR. Only MUs with clearly separable discharges from the crosstalk of other MUs have been kept for further analysis. It has been recently demonstrated, that in isometric contractions, an MU filter can be estimated from recordings during one contraction and applied to the recording of another contraction performed by the same muscle (31). Moreover, it was demonstrated that it is possible to track the same motor units in humans with HDsEMG under physiological conditions and following an intervention that reduced the motoneuron DR (33). We leveraged the characteristics of MU filters to track MUs between BR0 and BR21 (pre- to post-bedrest) at the same contraction intensity. We first applied the MU filters calculated from HDsEMG signals at BR0 to HDsEMG signals at BR21. This resulted in MU pulse trains estimated at BR21. We manually segmented these pulse trains into MU discharges, using the CKC Editor in the DEMUSE application. Afterward, the identified MU discharges were compared with the decomposition results from the standalone BR21 decomposition, calculating the Rate-of-Agreement (RoA) across all MU pairs from BR0 and BR21:

$$RoA = \frac{N_C}{C + N_{BR0 \to BR21} + N_{BR21}} \#$$

where N_C stands for the number of common MU discharges, identified after the MU filter transfer from BR0 to BR21 and in standalone BR21 decomposition and $N_{BR0 \to BR21}$ and N_{BR21} denote the number of MU discharges identified only from BR0 to BR21 MU filter transfer and from standalone BR21 decomposition, respectively. When calculating the RoA, the discharge match tolerance was set to 0.5 ms. The MUs identified in the standalone BR21 decomposition that exhibited $RoA \geq 30\%$ were considered tracked MUs. For these tracked MUs, discharges identified from standalone BR0 and BR21 decomposition were used for further analysis, whereas the discharges identified after the MU filter transfer were only used to calculate RoA and identify the same MU in BR0 and BR21.

From the identified MUs several parameters were computed using the *openhdemg* (v.0.1.0) Python (v.3.11, Python Software Foundation) package (34). First, the start and end of the steady-state contraction were manually marked to truly contain only the portion of the trapezoidal contraction where the force was steady. Then, the DR at recruitment and derecruitment was computed as the mean DR value of the first and last four discharges, respectively. The steady-state DR was calculated as the mean DR during the manually

Downloaded from journals.physiology.org/journal/jappl (193.002.022.014) on May 13, 2025.

defined steady part of the trapezoidal contraction, determined by visual inspection. Moreover, the first and last MU discharges were used to compute the relative recruitment thresholds as the relative force expressed as a percentage of the MVC at MU recruitment and derecruitment, respectively. Separate analyses were conducted for all detected MUs and for tracked MUs to evaluate changes at the population and individual MU levels.

iEMG signal decomposition and analysis

An expert operator (F.S.) employed the DQEMG software to automatically extract MU potential (MUP) trains from the steady-state of all 9 contractions (6 at 50% MVC and 3 at 50% MVC) and manually adjusted, where appropriate, the markers, relative to MUP onset, end, positive peak and negative peak (35). Inclusion criteria for MUP trains were: (i) more than 34 MUPs, (ii) signal-to-noise ratios >15 a.u., and (iii) MUP physiological shapes, as determined by the expert operator. Only MUP trains whose inter-discharge intervals followed a Gaussian distribution were considered for the DR analysis. We evaluated the following parameters (27, 36): MUP area and MUP duration, reflecting MU size, number of turns (i.e., a change in MUP waveform of at least 20 µV), indicative of the MUP complexity, and mean DR.

Additionally, the application of a second-order low-pass differentiator was employed to obtain the near-fiber MUPs (NFMs) trains (37), thereby focusing on the contribution of fibers located near the electrode recording surface (36). NFMs containing contaminating activity generated by other MUs were manually excluded. Only trains with >34 NFMs and with an NF peak count >1 were considered for data analysis. NMJ transmission was assessed using the NFM jiggle and NFM segment jitter, which represent the shape and temporal variability of consecutive NFMs, respectively (36).

2.7 Blood sampling and CAF analysis

Blood samples were obtained from the medial cubital vein at 7 a.m. with the participants in a fasted state. They were then centrifuged (centrifuge: CENTRIC 400, Domel, Železniki, Slovenia) at 2500 g (3880 rpm) for 10 min to separate serum from the other blood components. Samples were aliquoted and subsequently stored at −80°C until analysis. To investigate NMJ instability, serum C-terminal agrin fragment concentration (CAF) concentration was evaluated. An enzyme-linked immunosorbent assay (ELISA) analysis was carried out to analyze the serum concentration of CAF, using a commercially available kit

Downloaded from journals.physiology.org/journal/jappl (193.002.022.014) on May 13, 2025.

(Human Agrin SimpleStep ELISA, ab216945, Abcam, Cambridge, UK) and following the manufacturer's instructions. Samples were diluted 1:6 and run in duplicate. Standard curves were generated using known, increasing concentrations of CAF and measured at 450 nm. Sample CAF concentrations were determined by interpolation from the standard curves and corrected for dilution. The measurements demonstrated a coefficient of variation (CV) of less than 2%.

2.7 Muscle Biopsy

An expert clinician (M.G.) obtained a vastus lateralis muscle biopsy (∼150 mg) from each participant using a Weil–Blakesley conchotome (Gebrüder Zepf Medizintechnik GmbH & Co. KG, Dürbheim, Germany). To increase the likelihood of finding NMJ-positive tissue, each biopsy was performed at ∼2 cm proximally to the central innervation zone of the vastus lateralis (approximately at mid-thigh), an approach inspired by the recently introduced BeeNMJ method (38). Local anesthesia was administered using 2% lidocaine. The biopsy was divided into several portions, of which one (∼30 mg) was fixed in 4% paraformaldehyde and used in the present study.

Assessment of neuromuscular junction morphology

Muscle samples were dissected, cleared of fat and connective tissue, and separated into bundles of 3 to 5 fibers. To confirm the presence of NMJs, samples were incubated overnight with α-bungarotoxin conjugated to Alexa-555 (α-BTx Alexa-555 1:100, B35451, Life Technologies, California, USA) to label postsynaptic acetylcholine receptors (AChRs). Positive samples were then stained as follows: quenching with 50 mM ammonium chloride, permeabilization, and blocking (PBS with 2% BSA, 15% goat serum, 0.25% gelatin, 0.2% glycine, and 0.5% Triton X-100) for 2 hours. Primary antibody incubation was performed with antibodies against synaptic vesicle protein 2 (SV2; 1:200, Developmental Studies Hybridoma Bank, Iowa, USA) and against neurofilament (Nfl) heavy polypeptide (1:1000; Ab4680, Abcam, Cambridge, UK) for 4 days at +4°C. Secondary antibodies Alexa Fluor 647 (1:200; A-21235, Life Technologies, California, USA) were used along with α-BTx Alexa-555 (1:100) and secondary anti-chicken antibody conjugated with Alexa Fluor 488 (1:200; Ab150169, Abcam, Cambridge, UK). Samples were mounted using Fluorescent Mounting Medium (Dako Agilent, Santa Clara, CA, USA). Imaging was performed using a ZEISS LSM 900 confocal microscope with an Airyscan 2 detector and a 40x/1.4 oil immersion objective (Carl

Downloaded from journals.physiology.org/journal/jappl (193.002.022.014) on May 13, 2025.

Zeiss Microscopy, Jena, Germany). Laser power was optimized to prevent photobleaching, and excitation/emission settings were adjusted to minimize signal bleed-through. Multiple z-stacks were captured and collapsed into maximal intensity projections, which were analyzed using ImageJ (1.52v; National Institutes of Health, Bethesda, MD). NMJ occupancy was assessed using the Colocalization Threshold plugin in ImageJ (1.52v; National Institutes of Health, Bethesda, MD) to measure the overlap between the presynaptic terminal (stained by SV2) and the postsynaptic terminal (stained by α-bungarotoxin). NMJs were classified as denervated (<40% overlap), partially denervated (40–70% overlap), or innervated (>70% overlap), based on thresholds employed in our recent human study (39) that were adapted from previous rodent NMJ studies (40, 41). Nfl staining of axons was used only to distinguish between individual NMJs.

2.8 Statistical analysis

Two-tailed paired t-tests were employed to test differences between pre- and post-bed rest for the MVC, activation capacity, CSAs, and CAF. All these variables were normally distributed based on the Shapiro–Wilk test and visual inspection of Q–Q plots. Effects sizes were assessed using Hedges' g and interpreted as trivial ($g \geq 0.19$), small ($0.2 \leq g \leq 0.49$), medium ($0.50 \leq g \leq 0.79$), and large ($g \geq 0.80$) effects. For the HDsEMG and iEMG analysis, we carried out linear mixed models (fixed effect: time; cluster variable: subject), as multiple MUs are nested within each participant (42). As for iEMG parameters, the residuals of the models were not normally distributed, generalized linear mixed models were employed. The family of the distribution was the gamma or inverse Gaussian distribution, depending on each variable, with different associated link functions (Supplemental Table S1, available at https://doi.org/10.6084/m9.figshare.28769750). We employed minimal Bayesian information criterion (BIC) as the metric to compare the different models. Holm correction was applied for the post hoc comparisons. Statistical significance was set at $P < 0.05$. We employed repeated measures correlation to assess the within-individual association across the two time points using Python (Release 3.9.7; pingouin package; Python Software Foundation). We used *jamovi* software (v.2.3.21, Sydney, Australia) to carry out all the other statistical analyses and GraphPad Prism (v.8.00; GraphPad Software, San Diego, CA, USA) to create the graphs.

3. RESULTS

Downloaded from journals.physiology.org/journal/jappl (193.002.022.014) on May 13, 2025.

No side effects associated with bed rest exposure or the biopsy procedures were reported.

In vivo muscle morphology and function

As expected, the quadriceps CSA ($P < 0.001$; $g = 0.93$) and vastus lateralis CSA ($P < 0.001$; $g = 0.64$) were reduced at BR21 (Fig. 2D and E). A similar decreasing trend was observed for MVC ($P < 0.001$; $g = 1.63$). Strong repeated-measures correlations were observed between MVC and CSA for both vastus lateralis ($r=0.9$, $p=0.0004$) and whole quadriceps ($r=0.91$, $p=0.0003$). Specific tension was reduced following disuse (MVC/CSA) ($P = 0.007$; $g = 0.99$) (Fig. 2A and C). The activation capacity remained unchanged ($P = 0.135$; $g = 0.48$) (Fig. 2B).

Motor unit properties

In light of these functional changes, we wanted to determine whether neural control was altered following bed rest, evaluating MU properties at two different contraction intensities. The total number of MUs included in the study for both HDsEMG and iEMG is reported in Table 1. Details of the linear mixed models are reported in Supplemental Table S1 (available at https://doi.org/10.6084/m9.figshare.28769750).

Condition	***N. of participants***	***Total MUs***	***Total MUs divided per n. of contraction***	***Mean BR0 (per participant)***	***Mean BR21 (per participant)***
HDsEMG 25% MVC (Total MU Pool)	7	162	162	11.9 (6.49)	11.3 (6.75)
HDsEMG 50% MVC (Total MU Pool)	6	113	113	8.57(5.00)	8.83 (2.24)
HDsEMG 25% MVC (Tracked MU Pool)	7	102	102	7.29 (6.05)	7.29 (6.05)
HDsEMG 50% MVC (Tracked MU Pool)	6	50	50	4.17 (3.06)	4.17 (3.06)
iEMG 25% MVC (MUP)	8	550	92	35.5 (12.41)	33.25 (9.97)
iEMG 50% MVC (MUP)	6	149	50	12.67 (7.17)	12.17 (40.7)
iEMG 25% MVC (NFM)	8	321	54	19.63 (5.34)	20.5 (6.16)
iEMG 50% MVC (NFM)	6	83	28	6.17 (5.12)	7.67 (2.8)

Downloaded from journals.physiology.org/journal/jappl (193.002.022.014) on May 13, 2025.

Table 1: **Number of motor units (MUs) identified by high-density surface electromyography (HDsEMG) and intramuscular electromyography (iEMG) before (BR0) and after 21 days (BR21) of bed rest**. Some participants were excluded due to technical issues during the data collection or the absence of suitable MU potential trains. The number of tracked MUs assessed by HDsEMG coincides at BR0 and BR21 because the same MUs are monitored across both time points. iEMG outcomes are computed from all 9 contractions (6 at 25% and 3 at 50% of maximal voluntary contraction, MVC) with no duplicate removal, while HDsEMG outcomes contain only the contraction with the highest number of MUs sampled at each time point and contraction intensity. MUP: motor unit potential; NFM: near-fiber motor unit potential.

Results for the total pool and tracked pool of MUs assessed by HDsEMG are shown in Figs. 3 and 4. For both total and tracked MU pools, relative force at recruitment and derecruitment thresholds were not affected by bed rest at both contraction intensities, apart from an increase in recruitment threshold at 25% MVC on the total MU pool only ($P = 0.0467$).

DR derived from HDsEMG remained unchanged at recruitment and derecruitment but was reduced during the steady state, with total MUs pool (25% MVC: $P = 0.0057$; 50% MVC: $P = 0.0211$) and tracked pool (25% MVC: $P = 0.0481$; 50% MVC: $P = 0.0482$) exhibiting similar trend. To assess whether this pattern persisted when focusing exclusively on higher-threshold MUs, we repeated the analysis at 50% MVC including only MUs with recruitment thresholds >25% (19). We observed similar behavior in the total MU pool ($P = 0.021$), although this did not reach significance for the tracked pool ($P = 0.088$) (data not shown).

Reduced DR during the steady state was confirmed by iEMG (25% MVC: $P < 0.001$; 50% MVC: $P = 0.0266$) (Fig. 5).

Additionally, analysis of MU properties by iEMG (Fig. 6) revealed an increased number of MUP turns at both contraction intensities at BR21 (25% MVC: $P < 0.001$; 50% MVC: $P = 0.0315$), suggesting a greater MUP complexity induced by disuse. MUP area was decreased at 25% MVC ($P = 0.0015$) but increased at 50% MVC ($P = 0.0088$). MUP duration was increased only at 50% MVC ($P < 0.001$).

Neuromuscular junction function, instability, and morphology

We then focused more specifically on the NMJ, given its essential role in muscle contraction by transmitting electrical stimuli between motoneurons and muscle fibers. By iEMG, we observed an increase in NFM jiggle ($P = 0.0011$) at 25% MV, overall suggesting an impairment in NMJ transmission (Fig. 7). No changes in NFM segment jitter were observed.

Downloaded from journals.physiology.org/journal/jappl (193.002.022.014) on May 13, 2025.

Intrigued by this finding, we related this NMJ functional change to biochemical data, evaluating the serum concentration of CAF (Fig. 8A). We observed that CAF increased following bed rest ($P = 0.0056$; $g = 0.84$), suggesting indirectly NMJ instability with disuse (43). Finally, we attempted to evaluate directly the NMJ morphology from the muscle biopsies by whole-mount analysis. However, we identified only 4 participants with NMJ-positive samples at BR0 (168 NMJs in total) and 3 at BR21 (54 NMJs in total), with no participants matching between pre and post measurements, a known limitation of this complex approach (44). Given these issues, we did not perform a statistical analysis of the NMJ occupancy. From a qualitative point of view, it is interesting to note that the overlap between presynaptic and postsynaptic terminals was lower following bed rest (0.74 (0.04) at BR0 vs. 0.57 (0.19) at BR21; data not shown), with 15% of NMJs classified as denervated (overlap <40%) at BR21, whereas no denervated NMJs were observed at BR0 (Fig. 8B-D). These results should be considered complementary and interpreted with caution.

4. DISCUSSION

By combining iEMG, HDsEMG, and NMJ biological analysis, this study comprehensively evaluated changes at the MU level with medium-term muscle disuse in young individuals. The main findings are that 21 days of bed rest: (i) alters MU DR, MUP size, and MUP complexity at both low and moderate contraction intensities, (ii) impairs human NMJ transmission, and (iii) appears to trigger initial signs of NMJ instability and denervation.

Medium-term bed rest alters MU properties at both low and moderate contraction intensities

As expected, 21-day bed rest led to a marked reduction in muscle size (-11.9%) and force (-23.1%), with magnitudes consistent with estimates from meta-analyses (24, 45), supporting the effectiveness of the disuse model employed. This was accompanied by reductions in MU DR during the steady-state of low intensities contraction (25% MVC), in agreement with previous studies on shorter periods of muscle disuse (9, 17, 19). In addition, our study also detected similar reductions in DR at moderate contraction intensities (50% MVC), which contrasts with previous findings following 10 days of unilateral lower limb suspension (19). This pattern persisted when focusing exclusively on higher-threshold MUs, based on HDsEMG data. Thus, our findings suggest that longer periods of disuse may alter the activity

Downloaded from journals.physiology.org/journal/jappl (193.002.022.014) on May 13, 2025.

also of these MUs, ultimately leading to a DR reduction at 50% MVC. The findings on DR reduction were consistent across techniques (iEMG and HDsEMG), potentially suggesting that both superficial and deep MUs are affected uniformly by disuse. Motoneuron excitability and discharge properties are influenced by multiple intrinsic and extrinsic factors (46). Among these, one potential mechanism explaining declines in MU DR with disuse involves changes in persistent inward currents (PICs), which prolong and amplify the excitatory synaptic input to motoneurons and represent a major contributor to DR (47). We previously reported a reduction in estimated PICs assessed in the vastus lateralis following 10 days of unilateral lower limb suspension (48). Considering the longer disuse duration of the present study, and the consequential potentially greater unloading stimulus, the observed DR suppression could be driven by decreased neuromodulation. However, we cannot exclude also the possible contribution of motoneuron axonal structural damage, as this has been previously reported following periods of unloading in animal models (10, 11), and inferred indirectly in humans by increased concentrations of serum neurofilament light chain (9). However, these reductions in the DR occur in the absence of changes in neural strategies for activating and deactivating MUs under the same physiological conditions, as the relative forces at the recruitment and derecruitment thresholds were maintained in the tracked pool. This also implies that the recruitment order, governed by Henneman's size principle, remains intact following bed rest.

Employing iEMG, we noticed, at 25% MVC, a reduction in the MUP area, an index reflecting MUP size. Given this parameter is considered proportional to the size and number of fibers contributing to individual MUPs (49), this finding is a strong indication that myofibre atrophy may have occurred following bed rest. Although the increased MUP area at 50% MVC may initially seem surprising, we believe this reflects compensatory mechanisms, such as the recruitment of additional and/or larger MUs, to sustain the same relative moderate muscular effort. In addition, iEMG revealed an increased number of turns, reflecting an increased MUP complexity. While this was already shown with shorter disuse periods (10-15 days) at low contraction intensities (9, 17), to the best of our knowledge, this is the first study reporting this alteration also at higher MVC levels. Changes in MUP complexity in the context of disuse could be driven by initial denervation processes (13), and this possibility is supported by our NMJ morphology analysis (see below).

Downloaded from journals.physiology.org/journal/jappl (193.002.022.014) on May 13, 2025.

As changes in MVC exceeded those in MU properties this may suggest that, in addition to neural factors, other elements such as muscle atrophy (supported by our correlations between MVC and CSAs), reduced tendon stiffness (50), and intrinsic impairments in myofiber specific tension (6) likely contribute to disuse-induced muscle force loss.

On a technical note, the combination of iEMG and HDsEMG recordings offers significant advantages over applying the two techniques separately, providing unprecedented robustness to our results. Indeed, the application of iEMG overcomes the sensitivity of HDsEMG to the subcutaneous fat thickness and its bias towards superficial MUs (51), while also allowing the exploration of some parameters that are not currently validated by HDsEMG (MUP area, MUP turns, and NMJ-related parameters). On the other hand, the greater spatial resolution of HDsEMG and the ability to track the same MUs across different experimental sessions (52, 53) add a complementary dimension to our analysis. Our set-up, with the needle inserted at the matrix center, ensures great comparability between iEMG and HDsEMG results, as evidenced for instance by the similar declines of DR during the steady-state in response to disuse, observed with both techniques. Additionally, the greater axial distance between the needle insertion and the innervation zone (36 mm proximally) used in this set-up, compared to previous iEMG studies, may increase MU electrophysiological temporal dispersion (36), enhancing the ability to measure parameters related to MUP and NFM complexity and instability.

In summary, by combining iEMG and HDsEMG, we showed that medium-term bed rest impacts MU DR, MUP size, and MUP complexity in young individuals. As these alterations were observed at both 25% MVC and 50% MVC, an interpretation of these results is that also higher-threshold MUs are impacted by inactivity when the disuse period is prolonged.

Medium-term bed rest impairs neuromuscular junction transmission

Despite its fundamental role in neuromuscular function, there is limited literature on the alterations in NMJ transmission in response to inactivity. Pre-clinical studies in rodents showed changes in key proteins involved in neurotransmitter handling, as reviewed elsewhere (44), as well as changes in the acetylcholine quantal release (54–56). However, studies on humans are more controversial. Indeed, short-term disuse (10-15 days) does not impact iEMG parameters related to NMJ function in the vastus lateralis (9, 17), while another study in young and middle-aged adults reported alterations in the soleus after 28 days of cast immobilization (57). In the present study, we observed increased NFM jiggle,

Downloaded from journals.physiology.org/journal/jappl (193.002.022.014) on May 13, 2025.

along with a non-significant increase in NFM segment jitter, following 21 days of bed rest. These electrophysiological parameters are associated with the fluctuations in the time required for endplate potentials to reach the threshold necessary to generate muscle fiber action potentials (58). As such, they are considered proxies for the NMJ safety factor, the excess acetylcholine release ensuring reliable muscle contraction generation (59). As we previously hypothesized (9), our findings overall suggest that NMJ transmission impairments may develop only after medium-term disuse, whereas shorter periods of inactivity are likely insufficient to induce such alterations. While we observed this behavior only at 25% MVC, we believe this is primarily due to both the lower number of MUs included in the NFM analysis and the higher data variability observed at 50% MVC.

Medium-term bed rest might affect neuromuscular junction instability and structure

Although our primary focus was to study electrophysiological alterations, considering the impairment in NMJ transmission, we complemented our study with NMJ biochemical and morphological analyses. First, we observed an increased concentration of CAF, which may reflect increased NMJ instability (43). This finding aligns with our previous studies on shorter periods of disuse (10 days) across different unloading models (bed rest and unilateral lower limb suspension) (8, 9). However, as a circulating biomarker, CAF provides only an indirect evaluation of NMJ status (60). Similarly, previous literature has inferred early NMJ denervation with disuse indirectly at the muscle level, based on an increased percentage of neural cell adhesion molecule (NCAM) positive fibers (8, 9, 61, 62). To address this limitation, we conducted a morphological assessment of human NMJs from muscle biopsies with disuse. However, finding sufficient NMJ-positive samples is a relevant challenge of this approach (44), particularly in longitudinal studies. Given the small sample size (N=4 at BR0 with 168 NMJs; N=3 at BR21 with 54 NMJs) and the lack of participant matching (i.e., the analysis was conducted in samples from different participants between pre-to-post time points), our morphological results should be interpreted with caution and considered complementary. We observed the presence of denervated NMJs exclusively at BR21, suggesting that medium-term bed rest may trigger initial signs of denervation. These data align with the observed signs of NMJ denervation in rodents subjected to various disuse conditions (63, 64) and our recent data on a parallel 10-day bed rest study in older individuals (39).

Downloaded from journals.physiology.org/journal/jappl (193.002.022.014) on May 13, 2025.

In conclusion, 21-day bed rest induced alterations in MU electrophysiological properties, including reduced DR, changes in MUP size, and increased MUP complexity across low and moderate contraction intensities. We also observed impairment in NMJ transmission, accompanied by potential early signs of NMJ instability and denervation. Our findings suggest that disuse duration is a critical factor, as some of these alterations were not detected in previous studies using shorter time frames. Considering the small sample size, future studies are warranted to expand our findings in larger cohorts, including female participants.

SUPPLEMENTAL MATERIAL

Supplemental Table 1: https://doi.org/10.6084/m9.figshare.28769750.

DATA AVAILABILITY STATEMENT

The collection of z-stacks acquired in this study is openly available and can be accessed via the following link: https://osf.io/57ren/. This dataset includes all relevant images and data used in the analysis of NMJ morphology presented in this manuscript. The other data that support the findings of this study will be made available from the corresponding author upon reasonable request.

GRANTS

The present study was funded by the PRIN project ("InactivAge" n. 2020EM9A8X) and co-financed by the ARIS (project "J5-4593" and programme "P2-0041"). This study was also partly supported by the Space It Up project funded by the Italian Space Agency, ASI, and the Ministry of University and Research, MUR, under contract n. 2024-5-E.0 - CUP n. I53D24000060005. We also acknowledge co-funding from Next Generation EU (DM 1557 11.10.2022) to MVN in the context of the National Recovery and Resilience Plan, Investment PE8—Project Age-It: 'Ageing Well in an Ageing Society'. This work has received funding from the European Union's Horizon 2020 research and innovation programme under the Marie Skłodowska-Curie grant agreement 101034319 and from the European Union – NextGeneration EU. The views and opinions expressed are only those of the authors and do not necessarily reflect those of the European Union or the European Commission. Neither the European Union nor the European Commission can be held responsible for them.

ACKNOWLEDGEMENTS

Downloaded from journals.physiology.org/journal/jappl (193.002.022.014) on May 13, 2025.

The authors would like to thank Dr. Maira C. Scarpelli for her support with the MRI analysis, Dr. Matej Kramberger and Miss Katarina Puš for her help with data collection, and Prof. Marco Pirazzini, Prof. Ornella Rossetto, and Prof. Michela Rigoni for their supervision of the NMJ morphology analysis. The authors would also like to sincerely thank the volunteers for their time and effort in contributing to this study, as well as the staff of the Koper Science and Research Center (Institute for Kinesiology Research) for their essential support in organizing and assisting the participants throughout the study.

DISCLOSURES

The authors have no conflict of interest to declare.

AUTHOR CONTRIBUTIONS

F.S., M.K., E.S.M., G.D.V., A.H., B.S., R.P., and M.V.N. conceived and designed research; F.S., M.K., E.S.M., N.M., T.P., and M.G. performed experiments, F.S., M.K., E.S.M., M.V.F., N.M., G.V., and S.N. analyzed data; F.S., M.K., E.S.M., D.W.S., G.M., G.D.V., A.H., and M.V.N. interpreted results of experiments, F.S., M.K., and E.S.M. prepared figures; F.S. drafted manuscript; all the authors edited and revised manuscript; all the authors approved final version of manuscript.

REFERENCES

1. **Campbell M**, **Varley-Campbell J**, **Fulford J**, **Taylor B**, **Mileva KN**, **Bowtell JL**. Effect of Immobilisation on Neuromuscular Function In Vivo in Humans: A Systematic Review. *Sport. Med.* 49 Springer: 931–950, 2019.
2. **Hardy EJO**, **Inns TB**, **Hatt J**, **Doleman B**, **Bass JJ**, **Atherton PJ**, **Lund JN**, **Phillips BE**. The time course of disuse muscle atrophy of the lower limb in health and disease. *J Cachexia Sarcopenia Muscle* 13: 2616–2629, 2022. doi: 10.1002/jcsm.13067.
3. **Preobrazenski N**, **Seigel J**, **Halliday S**, **Janssen I**, **Mcglory C**. Single-leg disuse decreases skeletal muscle strength, size, and power in uninjured adults: A systematic review and meta-analysis. *J Cachexia Sarcopenia Muscle* 14: 684–696, 2023. doi: 10.1002/jcsm.13201.
4. **Hepple RT**, **Rice CL**. Innervation and neuromuscular control in ageing skeletal muscle. *J. Physiol.* 594 Blackwell Publishing Ltd: 1965–1978, 2016.
5. **Brocca L**, **Cannavino J**, **Coletto L**, **Biolo G**, **Sandri M**, **Bottinelli R**, **Pellegrino MA**. The time course of the adaptations of human muscle proteome to bed rest and the

Downloaded from journals.physiology.org/journal/jappl (193.002.022.014) on May 13, 2025.

underlying mechanisms. *J Physiol* 590: 5211–5230, 2012. doi: 10.1113/jphysiol.2012.240267.

6. **Trappe S**, **Creer A**, **Minchev K**, **Slivka D**, **Louis E**, **Luden N**, **Trappe T**. Human soleus single muscle fiber function with exercise or nutrition countermeasures during 60 days of bed rest. *Am J Physiol - Regul Integr Comp Physiol* 294: 939–947, 2008. doi: 10.1152/ajpregu.00761.2007.
7. **Murgia M**, **Ciciliot S**, **Nagaraj N**, **Reggiani C**, **Schiaffino S**, **Franchi M V**, **Pišot R**, **Šimunič B**, **Toniolo L**, **Blaauw B**, **Sandri M**, **Biolo G**, **Flück M**, **Narici M V**, **Mann M**. Signatures of muscle disuse in spaceflight and bed rest revealed by single muscle fiber proteomics. *PNAS Nexus* : 1–14, 2022. doi: 10.1093/pnasnexus/pgac086.
8. **Monti E**, **Reggiani C**, **Franchi M V**, **Toniolo L**, **Sandri M**, **Armani A**, **Zampieri S**, **Giacomello E**, **Sarto F**, **Sirago G**, **Murgia M**, **Nogara L**, **Marcucci L**, **Ciciliot S**, **Šimunic B**, **Pišot R**, **Narici M V**. Neuromuscular junction instability and altered intracellular calcium handling as early determinants of force loss during unloading in humans. *J Physiol* 599: 3037–3061, 2021. doi: 10.1113/JP281365.
9. **Sarto F**, **Stashuk DW**, **Franchi M V**, **Monti E**, **Zampieri S**, **Valli G**, **Sirago G**, **Candia J**, **Hartnell LM**, **Paganini M**, **Mcphee J**, **Vito G De**, **Ferrucci L**, **Reggiani C**, **Narici M V**. Effects of short-term unloading and active recovery on human motor unit properties, neuromuscular junction transmission and transcriptomic profile. *J Physiol* 600: 4731–4751, 2022. doi: 10.1113/JP283381.
10. **De-Doncker L**, **Kasri M**, **Falempin M**. Soleus motoneuron excitability after rat hindlimb unloading using histology and a new electrophysiological approach to record a neurographic analogue of the H-reflex. *Exp Neurol* 201: 368–374, 2006. doi: 10.1016/j.expneurol.2006.04.021.
11. **Canu MH**, **Carnaud M**, **Picquet F**, **Goutebroze L**. Activity-dependent regulation of myelin maintenance in the adult rat. *Brain Res* 1252: 45–51, 2009. doi: 10.1016/j.brainres.2008.10.079.
12. **Sarto F**, **Valli G**, **Monti E**. Motor units alterations with muscle disuse: what is new? *J Physiol* 600: 4811–4813, 2022. doi: 10.1113/JP283868.
13. **Piasecki M**. Motor unit adaptation to disuse: crossing the threshold from firing rate suppression to neuromuscular junction transmission. *J Physiol* 0: 1–9, 2024. doi: 10.1113/JP284159.

Downloaded from journals.physiology.org/journal/jappl (193.002.022.014) on May 13, 2025.

14. **Duchateau J**, **Hainaut K**. Effects of immobilization on contractile properties, recruitment and firing rates of human motor units. *J Physiol* 422: 55–65, 1990. doi: 10.1113/jphysiol.1990.sp017972.

15. **Seki K**, **Taniguchi Y**, **Narusawa M**. Effects of joint immobilization on firing rate modulation of human motor units. *J Physiol* 530: 507–519, 2001. doi: 10.1111/j.1469-7793.2001.0507k.x.

16. **Seki K**, **Kizuka T**, **Yamada H**. Reduction in maximal firing rate of motoneurons after 1-week immobilization of finger muscle in human subjects. *J Electromyogr Kinesiol* 17: 113–120, 2007. doi: 10.1016/j.jelekin.2005.10.008.

17. **Inns TB**, **Bass JJ**, **Edward JOH**, **Wilkinson DJ**, **Stashuk DW**, **Atherton PJ**, **Phillips BE**, **Piasecki M**. Motor unit dysregulation following 15 days of unilateral lower limb immobilisation. *J Physiol* 600: 4753–4769, 2022.

18. **Divjak M**, **Sedej G**, **Murks N**, **Gerževič M**, **Marusic U**, **Pišot R**, **Šimunič B**, **Holobar A**. Inter-Person Differences in Isometric Coactivations of Triceps Surae and Tibialis Anterior Decrease in Young, but Not in Older Adults After 14 Days of Bed Rest. *Front Physiol* 12: 1–14, 2022. doi: 10.3389/fphys.2021.809243.

19. **Valli G**, **Sarto F**, **Casolo A**, **Vecchio A Del**, **Franchi M V**, **Narici M V**, **Vito G De**. Lower limb suspension induces threshold-specific alterations of motor units properties that are reversed by active recovery. *J Sport Heal Sci* 13: 264–276, 2024.

20. **Škarabot J**, **Brownstein CG**, **Casolo A**, **Del Vecchio A**, **Ansdell P**. The knowns and unknowns of neural adaptations to resistance training. *Eur J Appl Physiol* 121: 675–685, 2021. doi: 10.1007/s00421-020-04567-3.

21. **Zero AM**, **Kirk EA**, **Hali K**, **Rice CL**. Firing rate trajectories of human motor units during isometric ramp contractions to 10, 25 and 50% of maximal voluntary contraction. *Neurosci Lett* 762: 136118, 2021. doi: 10.1016/j.neulet.2021.136118.

22. **Avrillon S**, **Hug F**, **Enoka R**, **Caillet AH**, **Farina D**. The decoding of extensive samples of motor units in human muscles reveals the rate coding of entire motoneuron pools. *Elife* 13: RP97085, 2024.

23. **Roach REJ**, **Cannegieter SC**, **Lijfering WM**. Differential risks in men and women for first and recurrent venous thrombosis: The role of genes and environment. *J Thromb Haemost* 12: 1593–1600, 2014. doi: 10.1111/jth.12678.

24. **Marusic U**, **Narici M**, **Simunic B**, **Pisot R**, **Ritzmann R**. Nonuniform loss of muscle

Downloaded from journals.physiology.org/journal/jappl (193.002.022.014) on May 13, 2025.

strength and atrophy during bed rest: A systematic review. *J Appl Physiol* 131: 194–206, 2021. doi: 10.1152/japplphysiol.00363.2020.

25. **Botter A**, **Oprandi G**, **Lanfranco F**, **Allasia S**, **Maffiuletti NA**, **Minetto MA**. Atlas of the muscle motor points for the lower limb: Implications for electrical stimulation procedures and electrode positioning. *Eur J Appl Physiol* 111: 2461–2471, 2011. doi: 10.1007/s00421-011-2093-y.

26. **Piasecki M**, **Ireland A**, **Stashuk D**, **Hamilton-Wright A**, **Jones DA**, **McPhee JS**. Age-related neuromuscular changes affecting human vastus lateralis. *J Physiol* 594: 4525–4536, 2016. doi: 10.1113/JP271087.

27. **Sarto F**, **Franchi M V.**, **McPhee JS**, **Stashuk DW**, **Paganini M**, **Monti E**, **Rossi M**, **Sirago G**, **Zampieri S**, **Motanova ES**, **Valli G**, **Moro T**, **Paoli A**, **Bottinelli R**, **Pellegrino MA**, **De Vito G**, **Blau HM**, **Narici M V.** Neuromuscular impairment at different stages of human sarcopenia. *J Cachexia Sarcopenia Muscle* 15: 1797–1810, 2024. doi: 10.1002/jcsm.13531.

28. **Jones EJ**, **Piasecki J**, **Ireland A**, **Stashuk DW**, **Atherton PJ**, **Bethan E**, **Mcphee JS**, **Piasecki M**. Lifelong exercise is associated with more homogeneous motor unit potential features across deep and superficial areas of vastus lateralis. *Geroscience* 43: 1555–1565, 2021.

29. **Holobar A**, **Zazula D**. Multichannel Blind Source Separation Using Convolution Kernel Compensation. *IEEE Trans SIGNAL Process* 55: 4487–4496, 2007.

30. **Holobar A**, **Minetto MA**, **Farina D**. Accurate identification of motor unit discharge patterns from high-density surface EMG and validation with a novel signal-based performance metric. *J Neural Eng* 11, 2014. doi: 10.1088/1741-2560/11/1/016008.

31. **Francic A**, **Holobar A**. On the Reuse of Motor Unit Filters in High Density Surface Electromyograms Recorded at Different Contraction Levels. *IEEE Access* 9: 115227–115236, 2021. doi: 10.1109/ACCESS.2021.3104762.

32. **Del Vecchio A**, **Holobar A**, **Falla D**, **Felici F**, **Enoka RM**, **Farina D**. Tutorial: Analysis of motor unit discharge characteristics from high-density surface EMG signals. *J Electromyogr Kinesiol* 53, 2020. doi: 10.1016/j.jelekin.2020.102426.

33. **Goodlich BI**, **Del Vecchio A**, **Kavanagh JJ**. Motor unit tracking using blind source separation filters and waveform crosscorrelations: reliability under physiological and pharmacological conditions. *J Appl Physiol* 135: 362–374, 2023. doi:

Downloaded from journals.physiology.org/journal/jappl (193.002.022.014) on May 13, 2025.

10.1152/japplphysiol.00271.2023.

34. **Valli G**, **Ritsche P**, **Casolo A**, **Negro F**, **De Vito G**. Tutorial: Analysis of central and peripheral motor unit properties from decomposed High-Density surface EMG signals with openhdemg. *J Electromyogr Kinesiol* 74: 102850, 2024. doi: 10.1016/j.jelekin.2023.102850.

35. **Stashuk DW**. Decomposition and quantitative analysis of clinical electromyographic signals. *Med Eng Phys* 21: 389–404, 1999. doi: 10.1016/S1350-4533(99)00064-8.

36. **Piasecki M**, **Garnés-Camarena O**, **Stashuk DW**. Near-fiber electromyography. *Clin Neurophysiol* 132: 1089–1104, 2021. doi: 10.1016/j.clinph.2021.02.008.

37. **Stashuk DW**. Detecting single fiber contributions to motor unit action potentials. *Muscle and Nerve* 22: 218–229, 1999. doi: 10.1002/(SICI)1097-4598(199902)22:2<218::AID-MUS10>3.0.CO;2-S.

38. **Aubertin-leheudre M**, **Pion CH**, **Vallée J**, **Dec C**, **Marchand S**, **Morais JA**, **Bélanger M**, **Robitaille R**. Improved Human Muscle Biopsy Method To Study Neuromuscular Junction Structure and Functions with Aging. 75: 2098–2102, 2020. doi: 10.1093/gerona/glz292.

39. **Motanova E**, **Sarto F**, **Rigoni M**, **Stashuk DW**, **Narici M V**. Neuromuscular junction instability with inactivity: morphological and functional changes after 10 days of bed rest in older adults. *J Physiol* https://doi.org/10.1113/JP288448.

40. **Courtney NL**, **Mole AJ**, **Thomson AK**, **Murray LM**. Reduced P53 levels ameliorate neuromuscular junction loss without affecting motor neuron pathology in a mouse model of spinal muscular atrophy. *Cell Death Dis* 10, 2019. doi: 10.1038/s41419-019-1727-6.

41. **Ang STJ**, **Crombie EM**, **Dong H**, **Tan KT**, **Hernando A**, **Yu D**, **Adamson S**, **Kim S**, **Withers DJ**, **Huang H**, **Tsai SY**. Muscle 4EBP1 activation modifies the structure and function of the neuromuscular junction in mice. *Nat Commun* 13: 1–15, 2022. doi: 10.1038/s41467-022-35547-0.

42. **Yu Z**, **Guindani M**, **Grieco SF**, **Chen L**, **Holmes TC**, **Xu X**. Beyond t test and ANOVA: applications of mixed-effects models for more rigorous statistical analysis in neuroscience research. *Neuron* 110: 21–35, 2022.

43. **Monti E**, **Sarto F**, **Sartori R**, **Zanchettin G**, **Lö S**, **Kern H**, **Narici MV**, **Zampieri S**. C-terminal agrin fragment as a biomarker of muscle wasting and weakness: a narrative

Downloaded from journals.physiology.org/journal/jappl (193.002.022.014) on May 13, 2025.

review. *J Cachexia Sarcopenia Muscle* 14: 730–744, 2023. doi: 10.1002/jcsm.13189.

44. **Motanova E**, **Pirazzini M**, **Negro S**, **Rossetto O**, **Narici M**. Impact of ageing and disuse on neuromuscular junction and mitochondrial function and morphology: Current evidence and controversies. *Ageing Res Rev* 102: 102586, 2024. doi: 10.1016/j.arr.2024.102586.

45. **Ruggiero L**, **Gruber M**. Neuromuscular mechanisms for the fast decline in rate of force development with muscle disuse – a narrative review. .

46. **Fuglevand AJ**, **Lester RA**, **Johns RK**. Distinguishing intrinsic from extrinsic factors underlying firing rate saturation in human motor units. *J Neurophysiol* 113: 1310–1322, 2015. doi: 10.1152/jn.00777.2014.

47. **Mesquita RNO**, **Taylor JL**, **Heckman CJ**, **Trajano GS**, **Blazevich AJ**. Persistent inward currents in human motoneurons: Emerging evidence and future directions. *J Neurophysiol* : 1278–1301, 2024. doi: 10.1152/jn.00204.2024.

48. **Martino G**, **Valli G**, **Sarto F**, **Franchi M V.**, **Narici M V.**, **De Vito G**. Neuromodulatory Contribution to Muscle Force Production after Short-Term Unloading and Active Recovery. *Med Sci Sports Exerc* 56: 1830–1839, 2024. doi: 10.1249/MSS.0000000000003473.

49. **Nandedkar SD**, **Sanders DB**, **Stälberg E V.**, **Andreassen S**. Simulation of concentric needle EMG motor unit action potentials. *Muscle Nerve* 11: 151–159, 1988. doi: 10.1002/mus.880110211.

50. **de Boer MD**, **Maganaris CN**, **Seynnes OR**, **Rennie MJ**, **Narici M V.** Time course of muscular, neural and tendinous adaptations to 23 day unilateral lower-limb suspension in young men. *J Physiol* 583: 1079–1091, 2007. doi: 10.1113/jphysiol.2007.135392.

51. **Merletti R**, **Muceli S**. Tutorial. Surface EMG detection in space and time: Best practices. *J Electromyogr Kinesiol* 49: 102363, 2019. doi: 10.1016/j.jelekin.2019.102363.

52. **Maathuis EM**, **Drenthen J**, **van Dijk JP**, **Visser GH**, **Blok JH**. Motor unit tracking with high-density surface EMG. *J Electromyogr Kinesiol* 18: 920–930, 2008. doi: 10.1016/j.jelekin.2008.09.001.

53. **Martinez-Valdes E**, **Negro F**, **Laine CM**, **Falla D**, **Mayer F**, **Farina D**. Tracking motor units longitudinally across experimental sessions with high-density surface

Downloaded from journals.physiology.org/journal/jappl (193.002.022.014) on May 13, 2025.

electromyography. *J Physiol* 595: 1479–1496, 2017. doi: 10.1113/JP273662.

54. **Robbins N**, **Fischbach GD**. Effect of chronic disuse of rat soleus neuromuscular junctions on presynaptic function. *J Neurophysiol* 34: 570–577, 1971. doi: 10.1152/jn.1971.34.4.562.
55. **Snider WD**, **Harris G**. A physiological correlate of disuse-induced sprouting at the neuromuscular junction. *Nature* 281: 70–71, 1979.
56. **Tsujimoto T**, **Kuno M**. Calcitonin gene-related peptide prevents disuse-induced sprouting of rat motor nerve terminals. *J Neurosci* 8: 3951–3957, 1988. doi: 10.1523/jneurosci.08-10-03951.1988.
57. **Grana EA**, **Chiou-Tan F**, **Jaweed MM**. Endplate dysfunction in healthy muscle following a period of disuse. *Muscle and Nerve* 19: 989–993, 1996. doi: 10.1002/(SICI)1097-4598(199608)19:8<989::AID-MUS6>3.0.CO;2-4.
58. **Juel VC**. Evaluation of neuromuscular junction disorders in the electromyography laboratory. *Neurol Clin* 30: 621–639, 2012. doi: 10.1016/j.ncl.2011.12.012.
59. **Wood SJ**, **Slater CR**. Safety factor at the neuromuscular junction. *Prog Neurobiol* 64: 393–429, 2001. doi: 10.1016/S0301-0082(00)00055-1.
60. **Jones RA**, **Ramadan A**, **Qutifan S**, **Gillingwater TH**. Comment on 'Neuromuscular Impairment at Different Stages of Human Sarcopenia' by Sarto et al. .
61. **Demangel R**, **Treffel L**, **Py G**, **Brioche T**, **Pagano AF**, **Bareille MP**, **Beck A**, **Pessemesse L**, **Candau R**, **Gharib C**, **Chopard A**, **Millet C**. Early structural and functional signature of 3-day human skeletal muscle disuse using the dry immersion model. *J Physiol* 595: 4301–4315, 2017. doi: 10.1113/JP273895.
62. **Arentson-Lantz EJ**, **English KL**, **Paddon-Jones D**, **Fry CS**. Fourteen days of bed rest induces a decline in satellite cell content and robust atrophy of skeletal muscle fibers in middle-aged adults. *J Appl Physiol* 120: 965–975, 2016. doi: 10.1152/japplphysiol.00799.2015.
63. **Fahim MA**. Rapid neuromuscular remodeling following limb immobilization. *Anat Rec* 224: 102–109, 1989. doi: 10.1002/ar.1092240113.
64. **Fahim MA**, **Kerdany MKE**. Disuse and functional overload induced by tooth extraction alters neuromuscular morphology in C57BL/6J mice. *Cell Mol Biol* 45: 401–5, 1999.

Downloaded from journals.physiology.org/journal/jappl (193.002.022.014) on May 13, 2025.

Figure captions:

Figure 1: **Schematic representation of the electromyography set-up.** To facilitate simultaneous intramuscular electromyography (iEMG) and high-density surface electromyography (HDsEMG) recordings, the HDsEMG matrix was incised at the center using a sterile scalpel, creating a small rectangular opening approximately 5 mm long and 3 mm wide (A). Data collection was performed on the vastus lateralis muscle during knee extensors' submaximal isometric contraction, with the concentric needle electrode inserted into the opening on the matrix (B). Participants were instructed to perform ramp trapezoidal contractions at 25% and 50% of their maximal voluntary contraction (MVC), with a ramp slope of 5% MVC/s. The steady-state phase duration was adjusted accordingly: 20 seconds at 25% MVC and 10 seconds at 50% MVC (C).

Figure 2: ***In vivo* muscle morphology and function before (BR0) and after 21 days (BR21) of bed rest**. Knee extensors' maximal voluntary contraction (MVC) (A), activation capacity (B), specific tension (C), quadriceps cross-sectional area (CSA) (D), and vastus lateralis CSA (E). Statistical analysis was performed using paired t-tests. Results are presented as mean values with individual data points displayed. N=9; one participant is missing from the activation capacity analysis due to discomfort experienced during the procedure. **$P < 0.01$; *** $P < 0.001$.

Figure 3: Recruitment strategies evaluated by high-density surface electromyography (HDsEMG), before (BR0) and after 21 days (BR21) of bed rest. Relative force at the recruitment threshold on the total motor unit (MU) pool (A), at the derecruitment threshold on the total MU pool (B), at the derecruitment threshold on the tracked MU pool (C), and at the derecruitment threshold on the tracked MU pool (D), expressed as a percentage of maximal voluntary contraction (MVC). Representative discharge rates recorded from the same participant at 25% MVC (E) and 50% MVC (F). Statistical analysis was performed using linear mixed models. Results are shown as estimated marginal mean (white dots) and 95% confidence intervals. N=7 for 25% MVC and N=6 for 50% MVC. *$P < 0.05$

Figure 4: Motor unit (MU) discharge rate (DR) assessed by high-density surface electromyography (HDsEMG) analyzed before (BR0) and after 21 days (BR21) of bed rest. DR at recruitment on the total MU pool (A), at derecruitment on the total MU pool (B), during the steady-state on the total MU pool (C), at recruitment on the tracked MU pool (D), at derecruitment on the tracked MU pool (E), and during the steady-state on the tracked MU pool (F). Data were collected during contractions at 25% and 50% of maximal voluntary contraction (MVC). Statistical analysis was performed using linear mixed models. Results are shown as estimated marginal mean (white dots) and 95% confidence intervals. N=7 for 25% MVC and N=6 for 50% MVC. *$P < 0.05$; **$P < 0.01$.

Figure 5: Motor unit (MU) discharge rate (DR) assessed intramuscular electromyography (iEMG) analyzed before (BR0) and after 21 days (BR21) of bed rest. DR during the steady-state (A), representative inter-discharge intervals distribution and DR recorded from the same participant at BR0 at 25% of maximal voluntary contraction (MVC) (B), at BR21 at 25% MVC (C), at BR0 at 50% MVC (D), and at BR21 at 50% MVC (E).

Downloaded from journals.physiology.org/journal/jappl (193.002.022.014) on May 13, 2025.

Statistical analysis was performed using generalized linear mixed models. Results are shown as estimated marginal mean (white dots) and 95% confidence intervals. BR0: blue dots; BR21: yellow dots. N=8 for 25% MVC and N=6 for 50% MVC. *P < 0.05; *** P < 0.001.

Figure 6: Motor unit potential (MUP) properties obtained using intramuscular electromyography before (BR0) and after 21 days (BR21) of bed rest. MUP area (A), MUP duration (B), MUP turns (C). Representative MUP templates recorded from the same participant at BR0 at 25% of maximal voluntary contraction (MVC) (D), at BR21 at 25% MVC (E), at BR0 at 50% MVC (F), and at BR21 at 50% MVC (G). MUP area is computed as the area under the MUP waveform displayed in blue; MUP duration was assessed as the time between markers 1 and 4; each MUP turn is highlighted by a magenta circle. Statistical analysis was performed using generalized linear mixed models. Results are shown as estimated marginal mean (white dots) and 95% confidence intervals. BR0: blue dots; BR21: yellow dots. N=8 for 25% MVC and N=6 for 50% MVC. *P < 0.05; **P < 0.01; ***P < 0.001.

Figure 7: Parameters associated with neuromuscular junction transmission, evaluated by intramuscular electromyography, before (BR0) and after 21 days (BR21) of bed rest. Near-fiber motor unit potential (NMF) jiggle (A); NFM segment jitter (B); and representative NFM shimmers at BR0 (C) and at BR21 (D) at 25% maximal voluntary contraction (MVC). Statistical analysis was performed using generalized linear mixed models. Results are shown as estimated marginal mean (white dots) and 95% confidence intervals. N=8 for 25% MVC and N=6 for 50% MVC. **P < 0.01.

Figure 8: Biochemical and morphological assessment of human neuromuscular junction (NMJ) before (BR0) and after 21 days (BR21) of bed rest. Serum C-terminal agrin fragment (CAF) concentration (A); NMJ occupancy analysis, reporting the percentage of innervated, partially denervated, and denervated NMJs (B). Representative NMJ morphology images at BR0 (C; overlap of 80%) and at BR21 (D; overlap of 25%). Acetylcholine receptors are displayed in magenta, while the synaptic vesicle protein 2 (SV2) in yellow. Statistical analysis was performed with a paired t-test (A), while we did not perform statistical analysis for (B) due to the low sample size and lack of participants matching. Results are presented as mean values with individual data points displayed (A). N=9 (A); N=4 at BR0 and N=3 at BR21 (B). **P < 0.01.

Downloaded from journals.physiology.org/journal/jappl (193.002.022.014) on May 13, 2025.

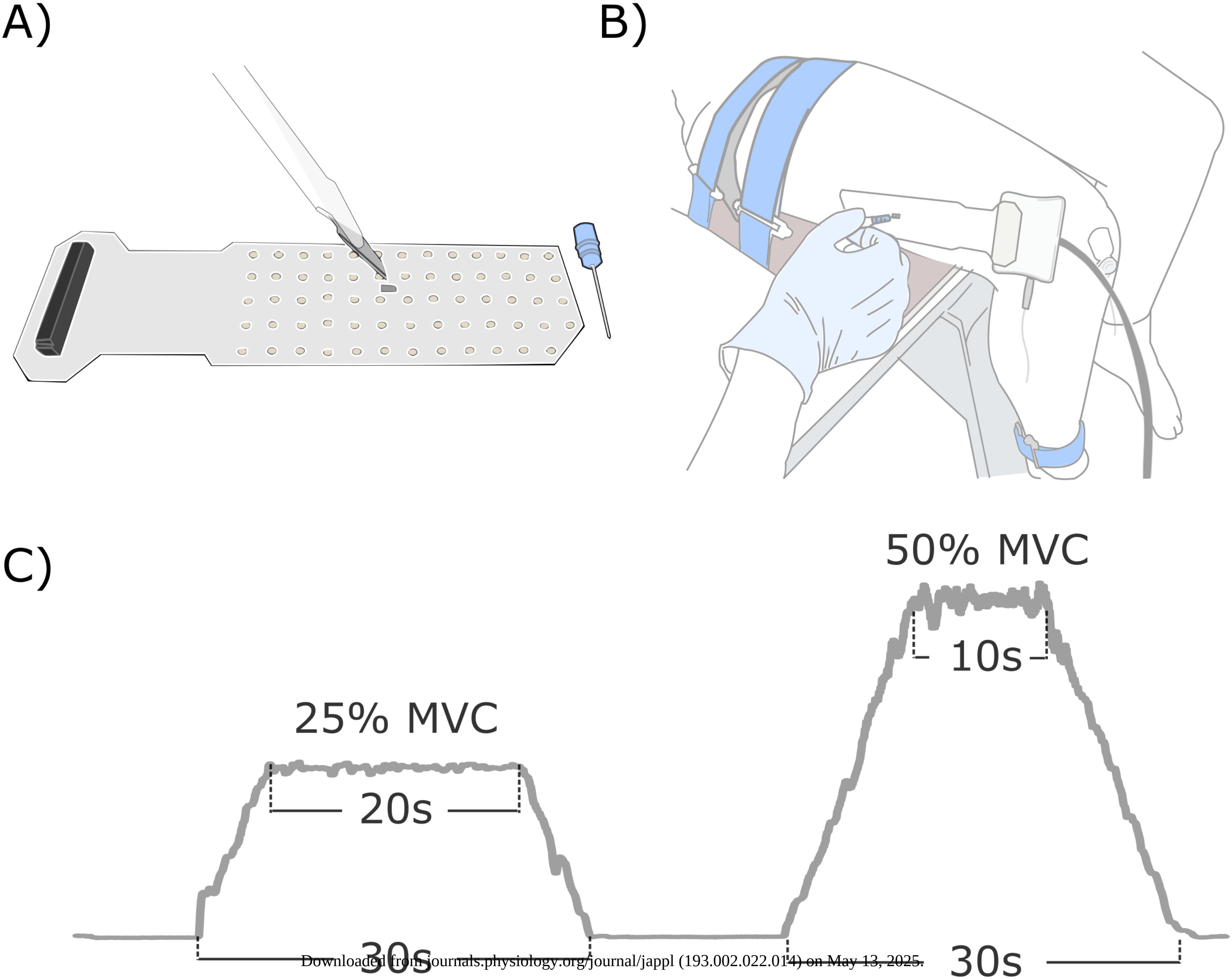

Downloaded from journals.physiology.org/journal/jappl (193.002.022.014) on May 13, 2025.

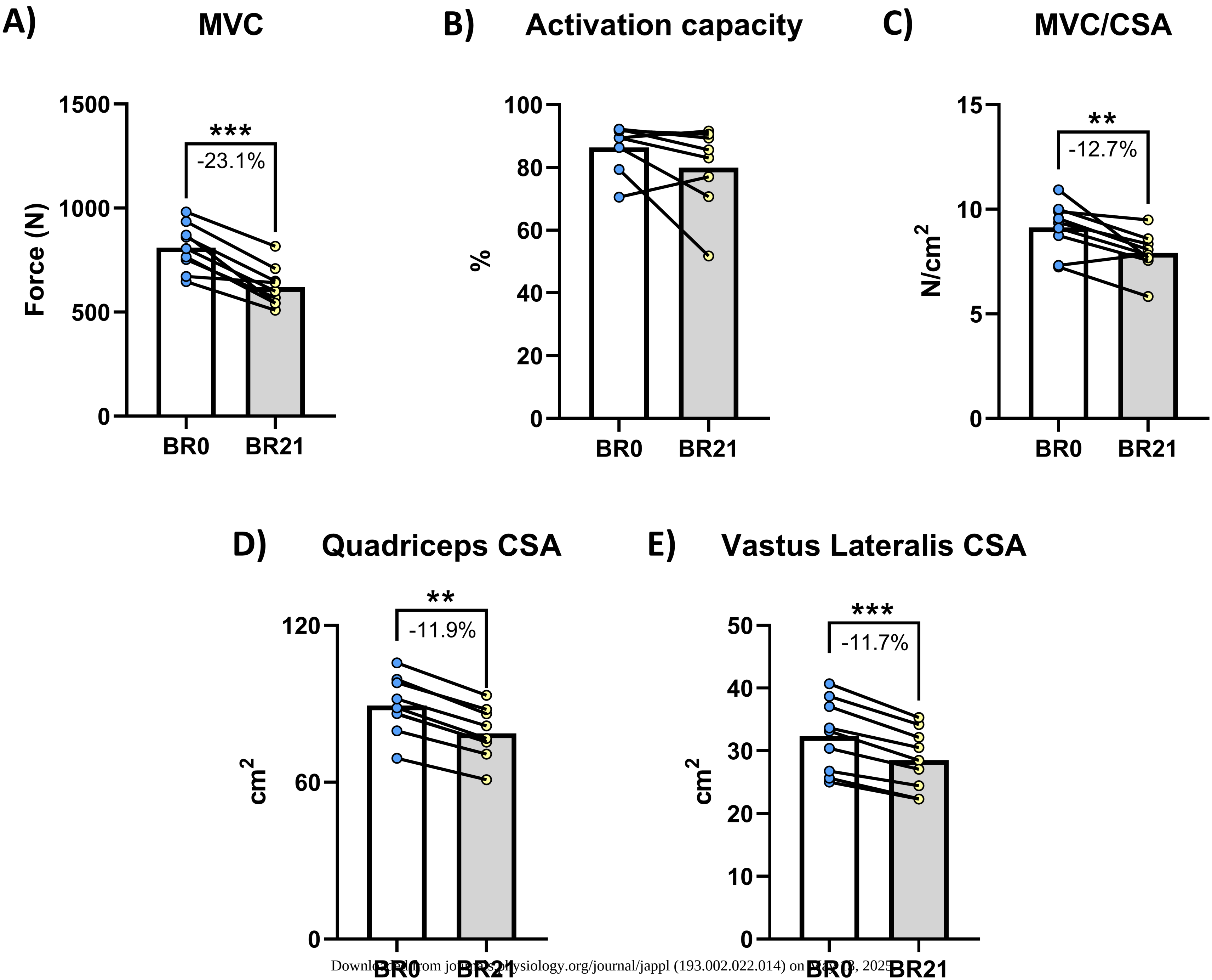

Downloaded from journals.physiology.org/journal/jappl (193.002.022.014) on May 13, 2025.

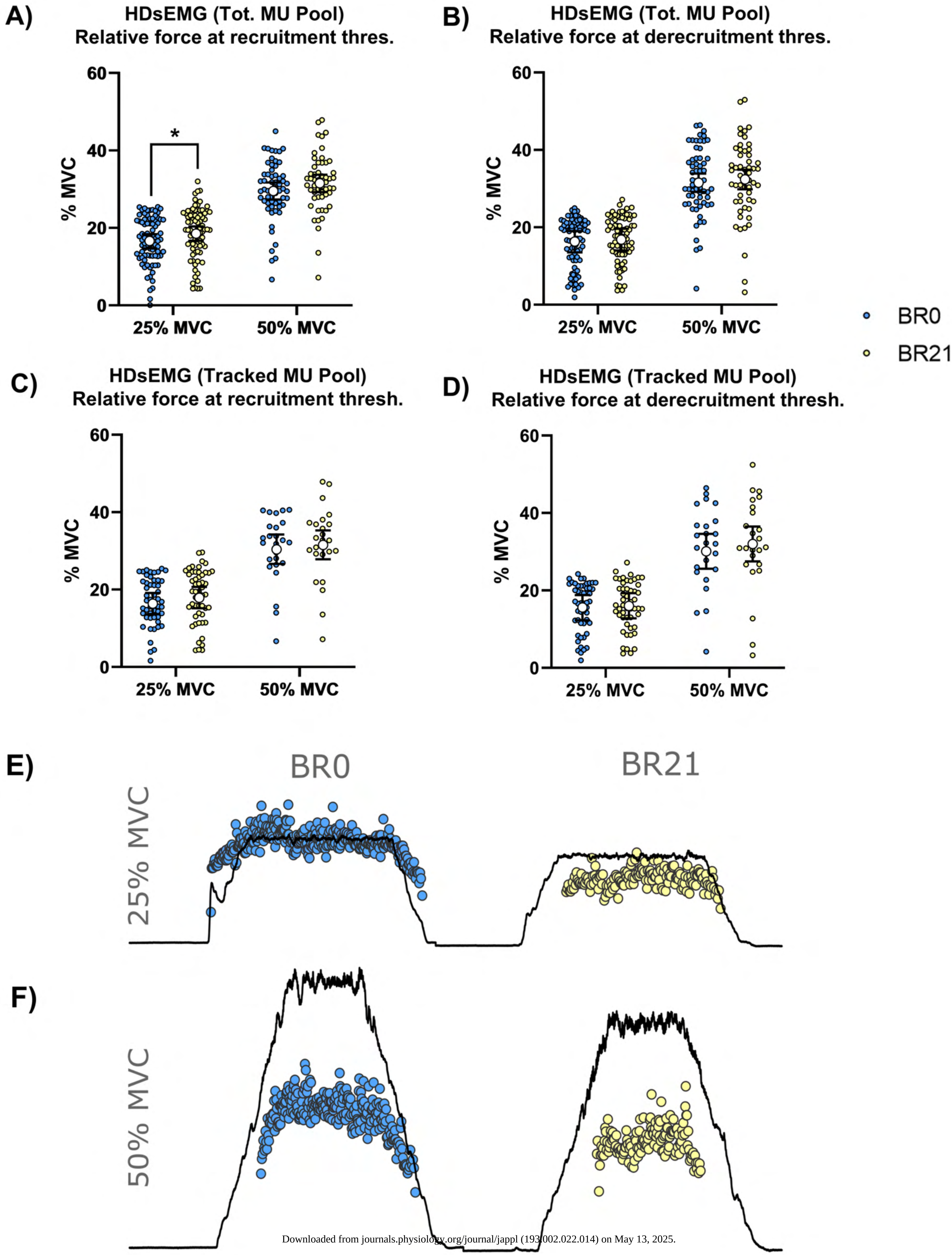

Downloaded from journals.physiology.org/journal/jappl (193.002.022.014) on May 13, 2025.

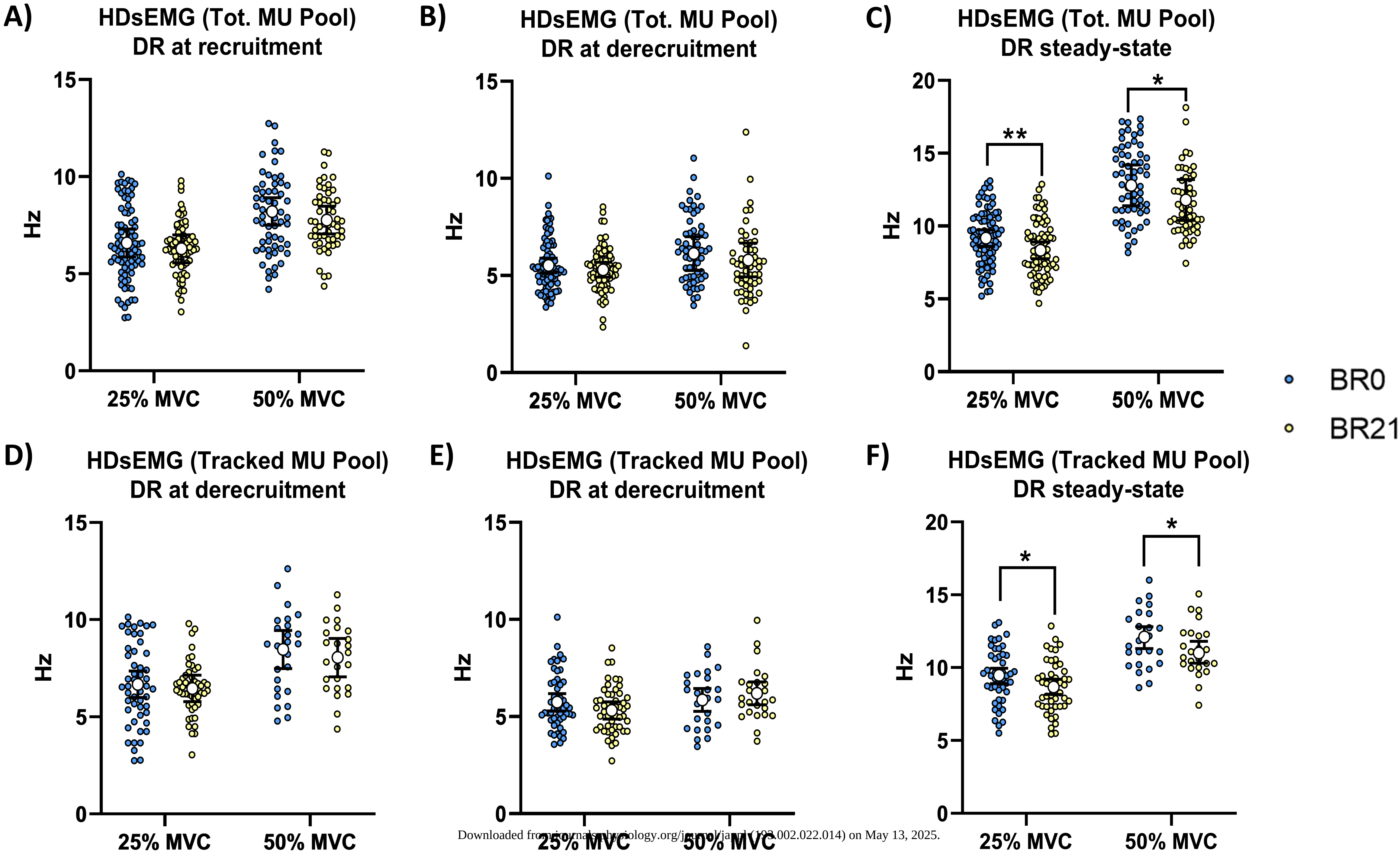

Downloaded from journals.physiology.org/journal/jappl (193.002.022.014) on May 13, 2025.

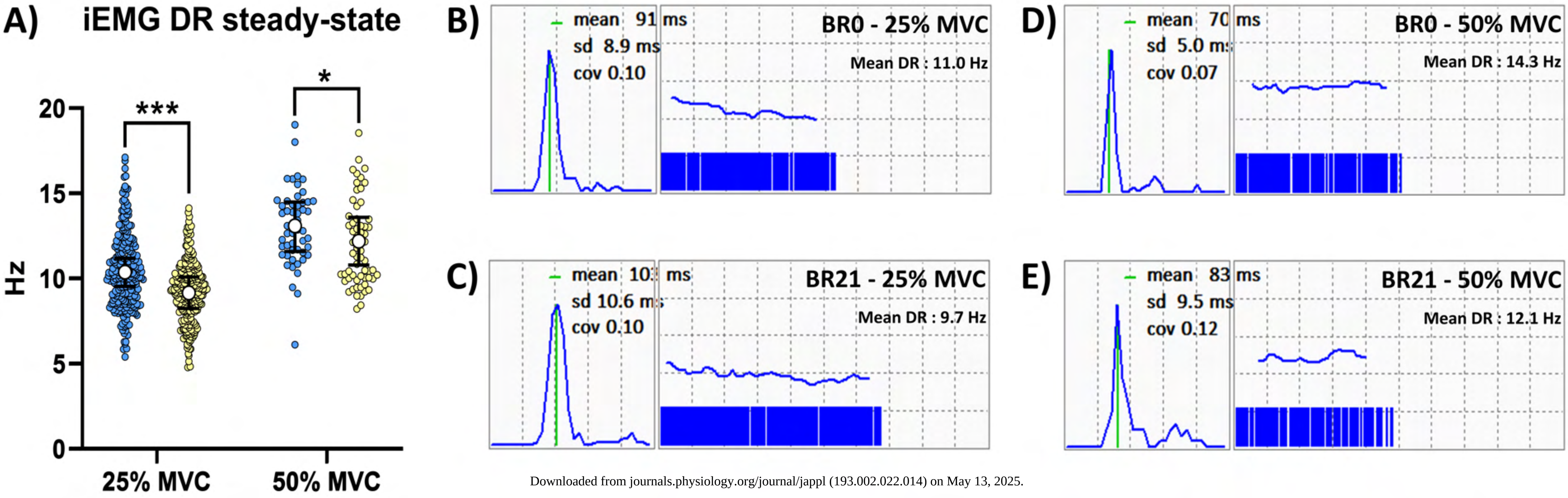

Downloaded from journals.physiology.org/journal/jappl (193.002.022.014) on May 13, 2025.

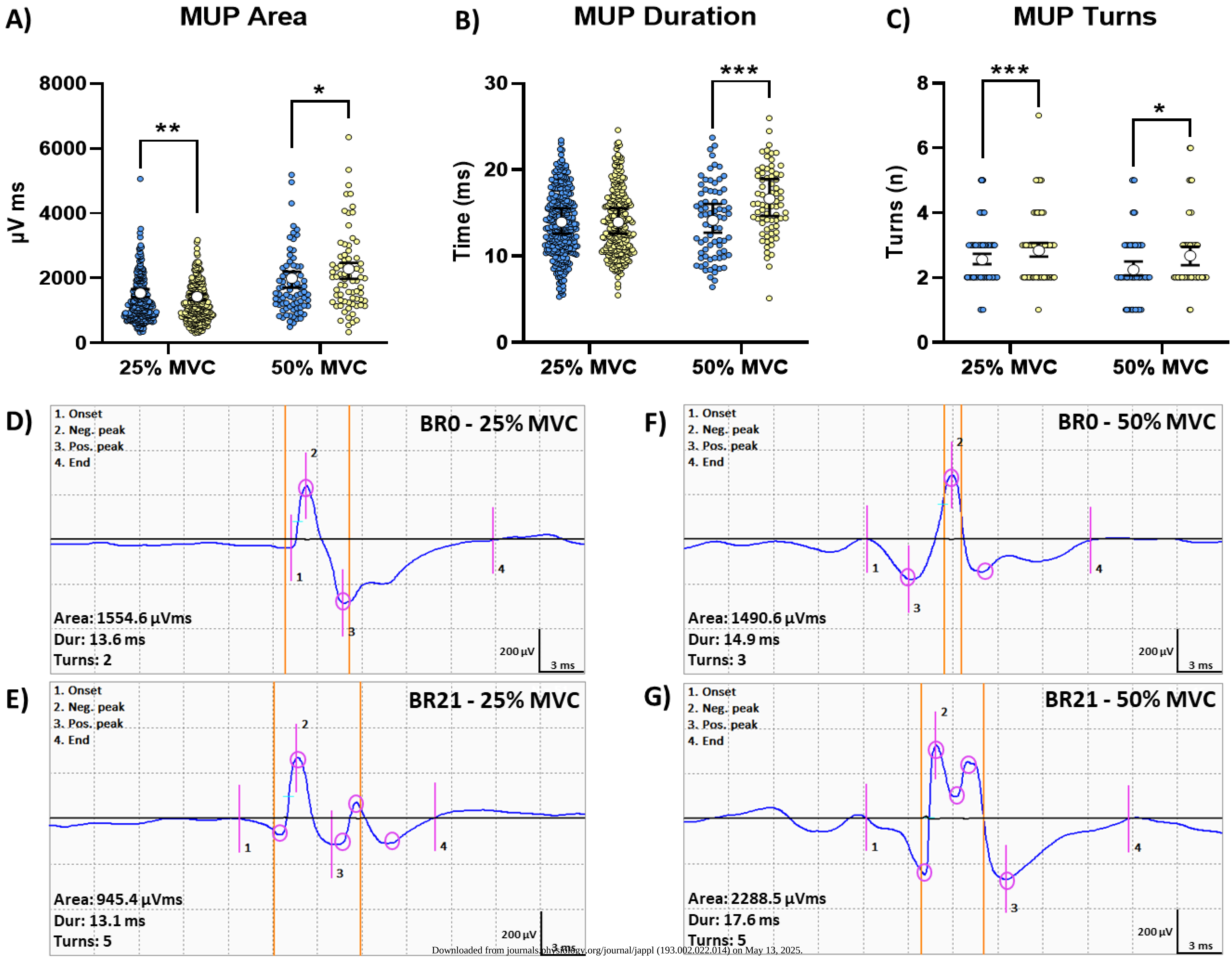

Downloaded from journals.physiology.org/journal/jappl (193.002.022.014) on May 13, 2025.

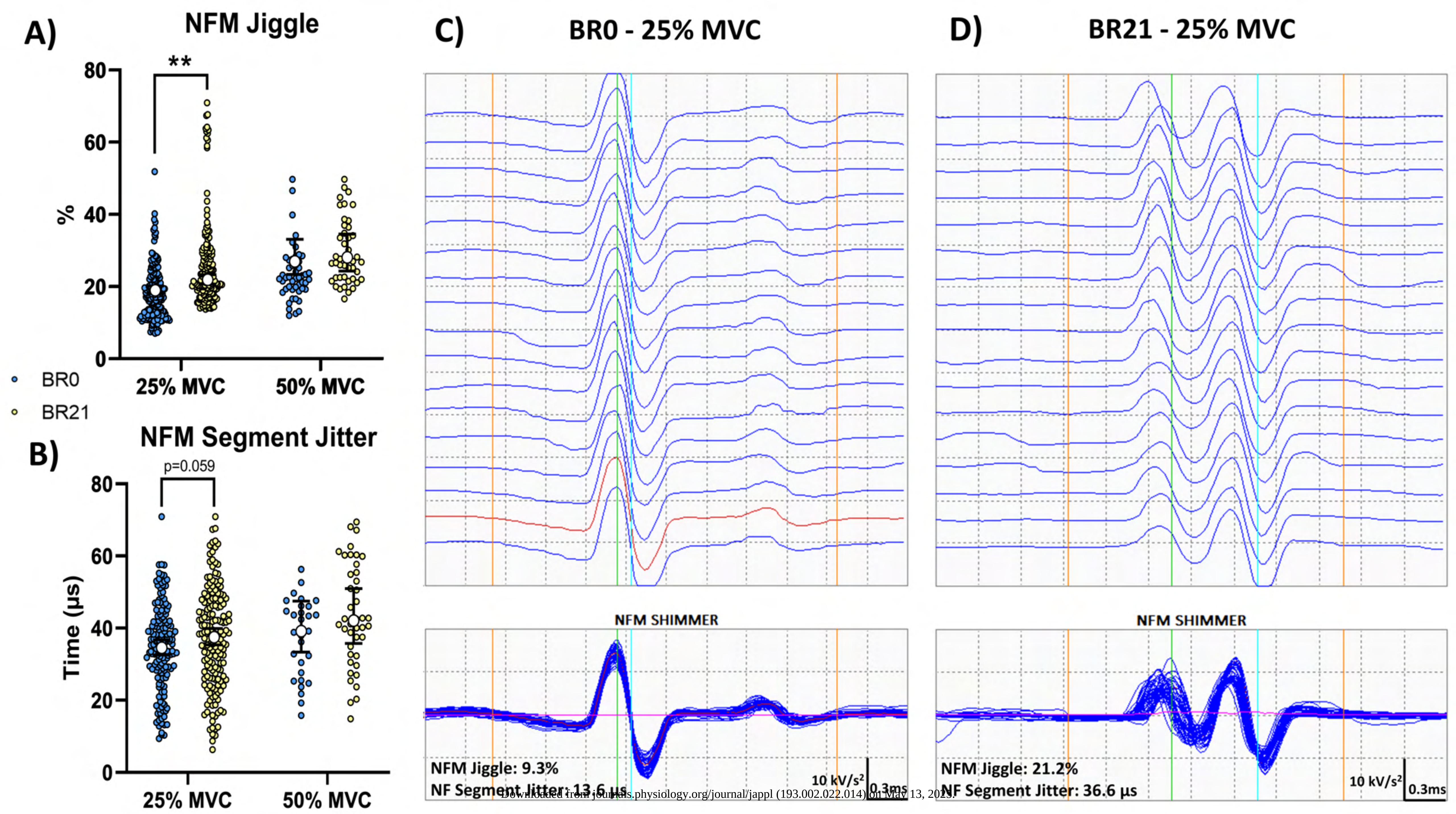

Downloaded from journals.physiology.org/journal/jappl (193.002.022.014) on May 13, 2023.

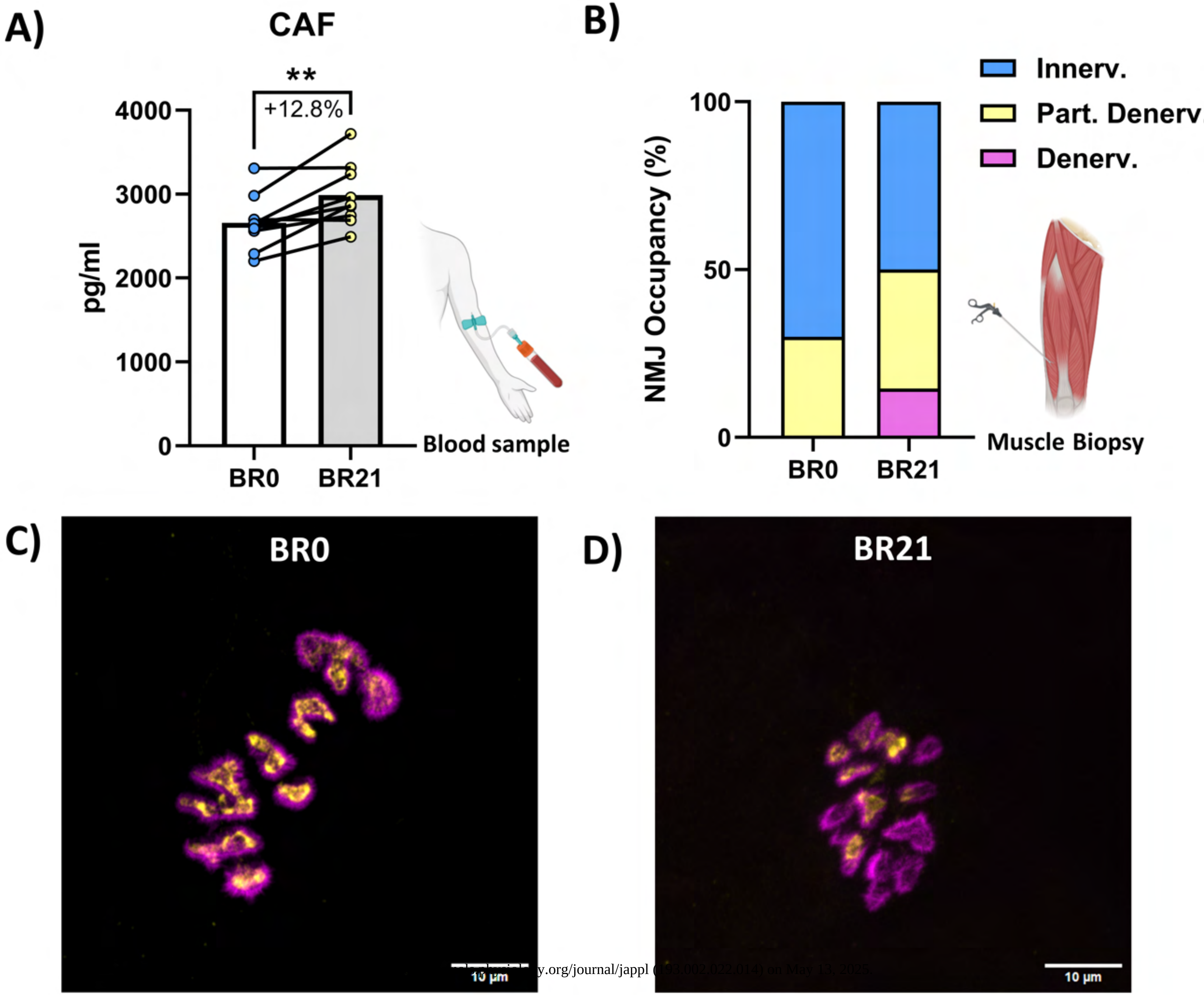

y.org/journal/jappl (193.002.022.014) on May 13, 2025.

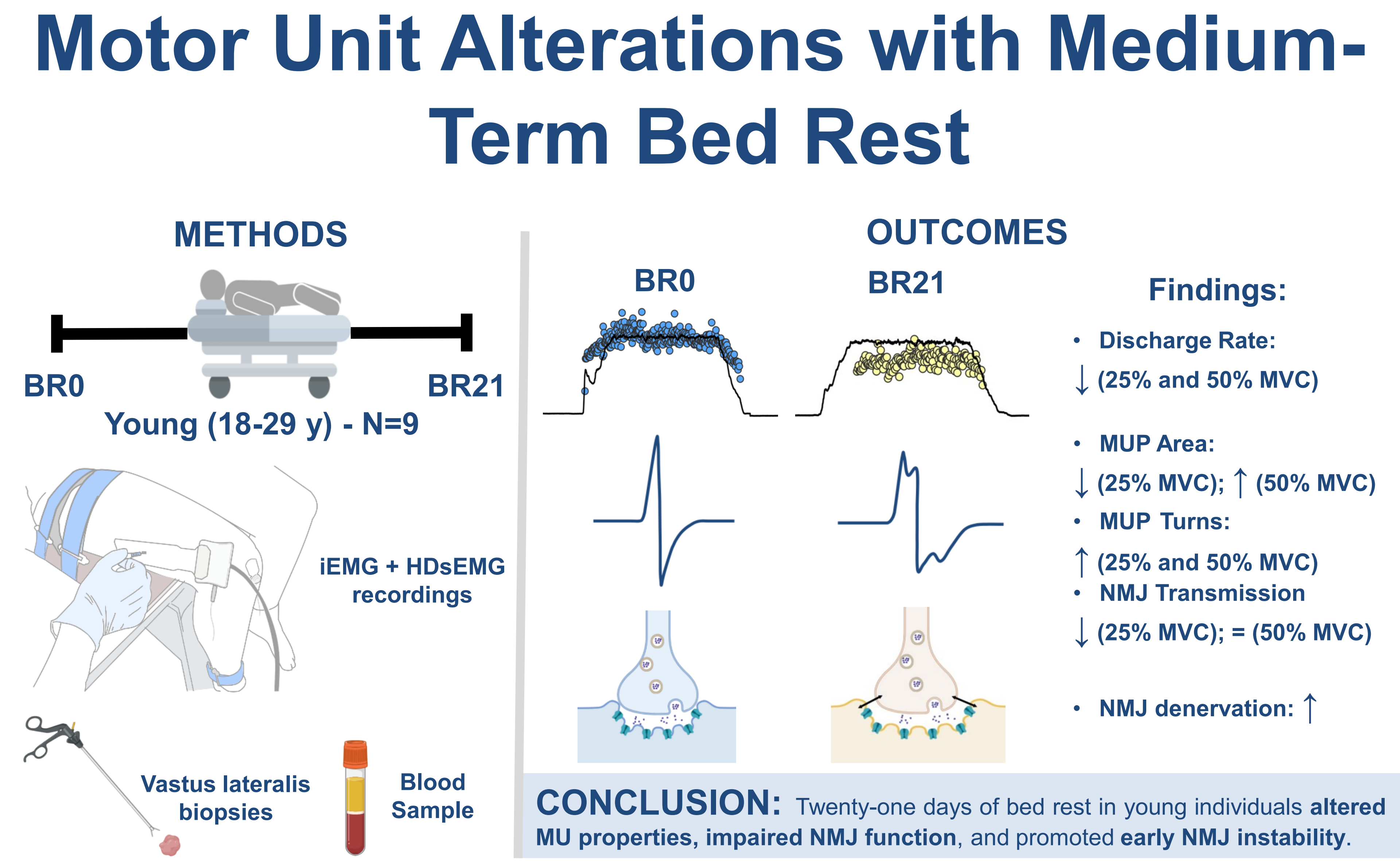

Downloaded from journals.physiology.org/journal/jappl (193.002.022.014) on May 13, 2025.